Influence of Solar Radiation on Classroom Environment in High Latitude and Rich Solar-Resource Areas

Jing Jiang[1], Dengjia Wang[1], Yanfeng Liu[1], Yaowen Chen[1] and Jiaping Liu[2]

[1] School of Environmental and Municipal Engineering, Xi'an University of Architecture and Technology, Xi'an (China)

[2] School of Architecture, Xi'an University of Architecture and Technology, Xi'an (China)

Abstract

Understanding of the knowledge of classroom temperature distribution is critical to design of solar system terminal. The temperature non-uniformity caused by solar radiation is not negligible, especially in high-latitude and strong radiation areas. This paper presents a detailed and comprehensive experiment in a primary and secondary school in northwestern China that was used to determine the thermal distribution and validate a simulation model. The temperature variations in both the vertical and horizontal directions were analyzed in detail. The indoor air temperature distribution was investigated with a systematic simulation of different conditions, including five solar radiation intensity levels, four southern external walls thicknesses and five window-to-wall area ratios. The results showed that the average air temperature difference in the vertical direction was nearly 3.0°C, whereas it was approximately 1.0°C in the horizontal direction. The optimal results of the non-uniform temperature distribution can provide the basis for determining the parameters of thermal design and heating system settings in primary and secondary school classrooms.

Keywords: Temperature distribution, simulation, classroom, non-uniform, in-situ measurement,

1. Introduction

Healthy and comfortable microclimate conditions are essential in any type of environment, but schools in particular are buildings, in which a high level of environmental quality can considerably improve attention, concentration, learning, listening and performance (Corgnati et al. 2007; Corrado and Astolfi, 2002).The need to provide good environments in commercial and educational buildings relies on the fact that people spend more than 90% of their time indoors. Students spend approximately 30% of their life in schools (Valeria et al. 2012), so researching the thermal environment in schools is essential. Existing research on indoor thermal environments has primarily focused on thermal comfort in the whole environment; information on indoor temperature distribution is limited, as current studies on indoor temperature distribution have concentrated on urban office and residential buildings (Srebric et al. 2008; Catalina et al. 2009). However, primary and secondary schools are different because students have a higher metabolic rate, classrooms have a higher density of personnel, and classroom time is relatively fixed. Thus, current distribution laws may not apply to primary and secondary school classrooms in northwestern China due to the unique indoor thermal environment requirements for students; it is essential that it need to study these temperature distributions.

Indoor temperature distribution is not only affected by interior personnel and equipment but also by factors such as wall thickness, materials and window-to-wall ratios etc. The latter factor is significantly influenced by solar radiation and other outdoor parameters. Because of economic underdevelopment, improving the indoor thermal environment of primary and secondary schools has primarily relied on renewable solar energy resources. This provides the basis and foundation for the study of classroom temperature distribution under different conditions for the construction of solar buildings.

Computational fluid dynamics (CFD) is a proven and effective simulation tool for predicting and analyzing buildings with reliable results. Building temperature and other parameters are strongly affected by the outdoor environment and the building envelope properties, which can be simulated and predicted using CFD (Desta and Janssens, 2004). Currently, CFD consistently provides a convenient method for indoor thermal environment evaluation and design for offices (Stamou and Katsiris, 2006), lecture halls(Cheng et al. 2003), and industrial

doi:10.18086/swc.2017.12.05 Available at http://proceedings.ises.org

premises (Rohdin and Moshfegh, 2007). Catalina (Catalina et al. 2009) showed test results for wall surface temperatures to be consistent with thermal boundary conditions. Rundle (Rundle et al. 2011) simulated indoor air temperature distribution given the temperature boundary condition of the outside wall surface and the heat flux boundary condition of the indoor heat source. In addition, because of the complex nature of windows, research has rarely considered the natural convection and radiation coupling of windows and the indoors. Behnia (Behnia et al. 1990) considered the effect of solar radiation and change of temperature inside the glass when modeling windows. Ismail (Ismail and Henriquez, 2003) simulated a corridor with a window inside of an air flow and temperature distribution and then analyzed the building energy consumption and use of solar energy. CFD is essential when studying the heat transfer properties of glass and room air flow and temperature effects.

A comprehensive test was conducted to determine the temperature distribution features of primary and secondary school classrooms with enriched solar energy resources in an actual passive solar classroom. On the basis of the actual test, temperature distribution is simulated through Fluent. There was a high degree of concurrence between the measured and the simulated results. The indoor air temperature distribution was investigated with a systematic simulation of different conditions, including different solar radiation intensity levels, southern external walls thicknesses levels and five window-to-wall area ratios. Therefore, the non-uniform characteristics of temperature change provided the foundation for the construction designs of solar buildings and system heating settings.

2. Methods

2.1. Experimental classroom

The experimental classroom was located in Huangzhong County (latitude:36°34′N, longitude:101°49′E, altitude: 2645m), Qinghai, China, where the average annual air temperature and precipitation were 5.1°C and 509.8mm, respectively, as provided by a meteorological station.

The experimental classroom is shown in Fig. 1. The east, west and north walls were constructed of 20 mm of plaster, 300 mm of aerated bricks, 20mm of polystyrene board and 20 mm of plaster. The roof and ground structures were constructed with 200 mm of steel-reinforced concrete and 50 mm of aerated concrete and 100 mm of poured concrete and 80mm of polystyrene board, respectively. The heat transfer coefficient of the windows was 1.1 (W m-2 K-1). The size of the south window was 2.3m×1.8m×2; the north window was 1.8m×0.9m×1.The north door was 2.1m high×0.9m wide in the front and back of the classroom.

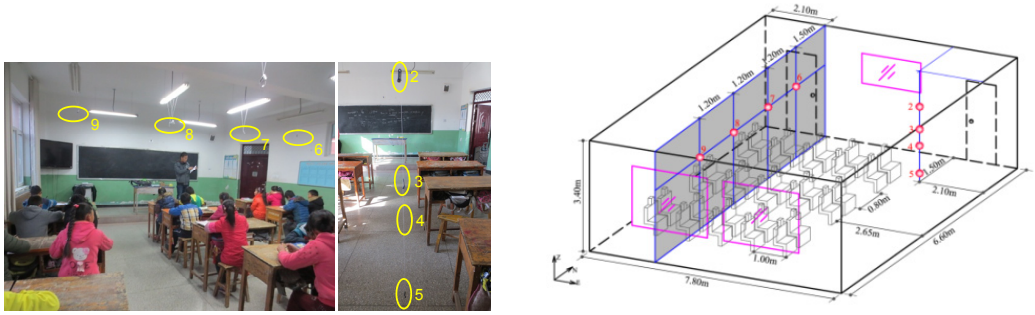

(a) Layout of experimental classroom (b) A real-scale 3-D model of the experimental classroom

Fig. 1: Measurement locations and dimensions of the experimental classroom

2.2. Measuring parameters, instruments and experimental procedure

The outdoor temperature and relative humidity were simultaneously measured according to the indoor classroom measurements by means of a portable automatic meteorological station located on the roof of the school building. The indoor environment measurements were automatically recorded every 10 minutes over 24h every day for a total of seven days (from 5 to 11 December 2015). Tab. 1 summarizes the characteristics of the equipment. The measurement equipment was fitted to the classroom to collect indoor environmental variables, such as air temperature, relative humidity, air velocity. The equipment was placed at eight locations inside the classroom and at one outdoor location without disturbing class activities and far from any heat sources, such as projectors or computers. The detailed measurement points are shown in Tab. 2 and correspond to Fig. 1.

Tab. 1: Measuring equipment specifications

Parameters	Instrument	Model	Accuracy	Operating method
Solar radiation intensity	Solar pyranometer	TBD-1	±8.789 W m^{-2}	Automatic recording every 10 min
Outdoor air temperature and relative humidity	Portable automatic meteorological station	Vantage Pro2	±0.5°C/±5%	
Indoor air temperature and relative humidity	Recording thermometer	TR-72U	±0.2°C/±5%	
Wall surface temperature	Thermocouple thermometer	CENTER309	±(0.3%rdg)+1°C	

Tab. 2: Measurement details of monitored positions at the cross-section shown in Fig. 1

Monitored position(P)	Measured items	Notes
1(Not shown)	Outdoor air temperature, Wind velocity, Solar radiation, etc.	Portable automatic meteorological station placed on roof (open space)
2	Indoor air temperature	Height:2.30m
3		Height:1.60m
4		Height:1.10m
5		Height:0.25m
6/7/8/9	Indoor air temperature	Height:2.30m

2.3. Computer simulation

Physical model. A real-scale 3-D model (shown in Fig. 1) of the experimental classroom was created with two modules: for fluid computational domains such as inside and outside air, and solid computational domains such as walls, roof and floor. Energy and Standard *k-ε* Turbulence Models were selected.

Model simplifications. 1) Humidity was not taken into consideration; 2) Air exchange between the inside and outside of the classroom was neglected because natural ventilation was negligible for the closed experimental classroom; and 3) The heat processes of the east wall, west wall and roof were considered to be adiabatic.

Governing equations. CFD is a numerical methodology that solves the governing equations of fluid flow by using a finite volume method to convert partial differential equations into a set of algebraic equations (Molina-Aiz et al. 2010; Zhang et al. 2016). It is based on the resolution of the governing equations of three conservation laws that include mass, energy, and momentum transport equations as follows (Versteeg and Malalasekera, 1995):

$$\frac{\partial(\rho\delta)}{\partial t} + div(\rho\mu\delta) = div(\Gamma_\delta \cdot grad\,\delta) + S_\delta \qquad \text{(eq. 1)}$$

where δ is the universal variable; ρ, μ, Γ_δ and S_δ are the density (kg m^{-1}), velocity vector (m s^{-1}), generalized diffusion coefficient (m^2 s^{-1}), and source term (W m^{-1}), respectively. This presents as a continuity equation when δ is 1, an energy equation when δ is T and a momentum equation when δ is u, v, w (m s^{-1}) with velocities in the directions of x, y, and z, respectively.

Initial and boundary conditions. Five types of boundary conditions were defined: the outside air temperature (T_{out}), the air temperature of the north corridor (T_c), the radiant sky temperature (T_{sky}), the surface convective heat transfer coefficient (h_o) and the soil surface temperature (T_f). The initial temperature of the inside air was set as an average value at 8:00 during the experimental period.

The air temperature (including T_{out} , T_c)changed over time; the conduction equation was solved inside the walls and can be fitted based on the experimental data during the entire day as follows:

$$T_{out} = 268.7 - 6.9 \times \cos(0.000073\tau + 5.2) \qquad R^2 = 0.9173 \qquad \text{(eq. 2)}$$

from 8:00(t=0 s $\tau = t + 3600 \times 8$) to 18:00(t=36000s)

$$T_c = 276.8 - 0.5 \times \cos\left(0.000073\tau - 26.3\right) \qquad R^2 = 0.7222 \qquad \text{(eq. 3)}$$

where τ is the time(s) and $28800 \le \tau \le 36000$; R^2 is the degree of fitting.

The heat transfer of the exterior wall can be determined by the convective heat transfer coefficient that can be calculated by eq. (4).

$$K_0 = \frac{1}{\frac{1}{h_i} + \sum \frac{d}{\lambda} + \frac{1}{h_o}} \qquad \text{(eq. 4)}$$

where K_0 is the heat transfer coefficient, W m^{-2} K^{-1}; h_i and h_o are the heat transfer coefficients of the inner and outer wall surfaces, respectively, W m^{-2} K^{-1}; d is the thickness of the wall, m; and λ is the thermal conductivity coefficient, W m^{-1} K^{-1}.

The thermal radiant exchange with the sky influences the heat balances of the exterior wall. It is therefore necessary to determine the radiant sky temperature T_{sky} (Tang et al. 2003). The following proposed empirical formula (Berdahl and Fromberg, 1982) was used:

$$T_{sky} = \varepsilon_{sky}^{0.25}\left(T_a + 273\right) \qquad \text{(eq. 5)}$$

$$\varepsilon_{sky} = 0.74 + 0.006T_{dp} \qquad \text{(eq. 6)}$$

where T_a is ambient air temperature, K.

The dew point temperature T_{dp} has the following empirical correction expressed in degrees Celsius(Cook,1985):

$$T_{dp} = 26.14 + 16.99C + 1.8893C^2 \qquad \text{(eq. 7)}$$

$$C = \ln\left(Rh \cdot Pa\right) = \ln\left(Rh\right) - 8.0929 + 0.97608\left(T_a + 42.607\right)^{0.5} \qquad \text{(eq. 8)}$$

where Rh is the relative humidity, %; and Pa is the saturation vapor pressure of the air at any air temperature.

The final fitting equation of T_{sky} is below:

$$T_{sky} = 276.8 - 6.8 \times \cos\left(0.000073\tau + 5.2\right) \qquad R^2 = 0.8498 \qquad \text{(eq. 9)}$$

To conveniently validate and utilize the established simulation model, the floor was regarded as playing a constant wall temperature role.

The evaluation of the metabolic rate in the school building was obtained from Havenith (Havenith, 2007), who studied the metabolic rate and clothing insulation of children and adolescents. The metabolic rate was set at 52 W m^{-2} in accordance with a simple writing task or sedentary activity. The total heat release of a human body was set at 76 W per person (Srebric et al. 2008). The temperature around the body was simulated by a given body surface heat flux.

2.4. Model applications

Once the computer simulation was validated, it was used to predict the thermal environment with different conditions in terms of varying solar radiation intensities, south external wall thicknesses and window-to-wall area ratios, as listed in Tab. 3. The same model parameters, initial and boundary conditions and solving methodology were used in all models.

Tab. 3: Different cases of different conditions for simulation

(a) Five cases of solar radiation intensity for simulation

Case	Solar radiation intensity level(W m^{-2})
1	800
2	600(Case validation)
3	400
4	200

5	100

(b) Four cases of thickness of the south wall for simulation

Case	Thickness of the south wall(mm)
1	240+20
2	370+20(Case validation)
3	520+20
4	630+20

(c) Four cases of window-to-wall area ratio for simulation

Case	Area ratio of window to wall	Length(m) × Width(m) × Number
1	0.3(Case validation)	2.3×1.8×2
2	0.4	2.4×2.4×2
5	0.5	2.8×2.5×2
3	0.6	3.0×2.8×2
4	0.7	3.2×3.2×2

3. Results and discussion

3.1. Measuring results and analysis

Ambient air conditions. Fig. 2 shows the indoor and outdoor air temperatures along with the solar radiation intensity for one measured day. During the day, the maximum global and direct radiation levels were 557 W m^{-2} and 470 W m^{-2}, respectively. The mean outdoor air temperature and relative humidity were -1.3°C and 54.6%, respectively. The air temperature ranged between 6.1°C and 13.4°C, with an average of 8.7°C during the day. The relative humidity ranged between 16% and 74% and the air velocity ranged from 0 to 0.49 m s^{-1}. However, the variations in global solar radiation, outdoor air temperature and indoor air temperature ranged from 0 to 557 W m^{-2}, from -6.2°C to 8.1°C, and from 6.1°C to 13.4°C, respectively, with averages of 284 W m^{-2}, 1.8°C and 10.8°C during the school day.

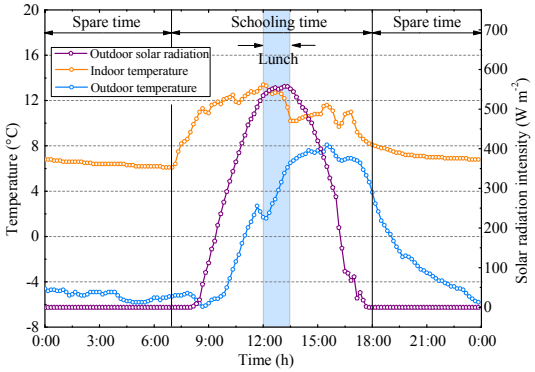

Fig. 2: Indoor and outdoor air temperatures and solar radiation intensity

Vertical temperature distribution. There are considerable differences in ambient building temperatures that also influence the distribution of temperature fields inside buildings. According to the measured temperature data, there was significant non-uniformity in the temperature field distribution inside the measured building. The uneven distribution of the temperature field was analyzed in the vertical and horizontal directions.

The temperature variation in the vertical direction is shown in Fig. 3(a). The building temperature field, as

observed in the temperature distribution, shows significant non-uniformity in the vertical direction. The measured temperature at 2.3 m was consistently higher than the other locations. The temperature at 1.6m was slightly higher than at 1.1m but substantially less than at 2.3 m. Obviously, the temperature is the lowest at ground level. It can be seen from the diagram that the change tendency of the four lines is roughly the same. The temperature decline was primarily due to students leaving the room for recess, lunch and nap. Heated air moves upward in the classroom, the heat loss of human body at 1.1~1.6m makes the temperature higher than at ground level (0.25m).

To facilitate analysis, the measured temperature data at representative timings (8:00, 10:30, 12:00, 12:30, 14:30, and 16:10) were selected for assessing non-uniformity. The temperature values at different points are shown in Fig. 3(b). It can be seen that the tendency of the temperature distribution was generally similar. The mean temperature during the school day (from 7:00 to 18:00) was calculated. In the range of 0.25 to 1.1m, the rate of temperature increase was greater due to the heat dissipation from the human bodies to the indoor environment at 2.0 °C m^{-1}. Because of the lower personnel density, the rate of temperature increase reached 0.8 °C m^{-1} at 1.1 to 1.6m.

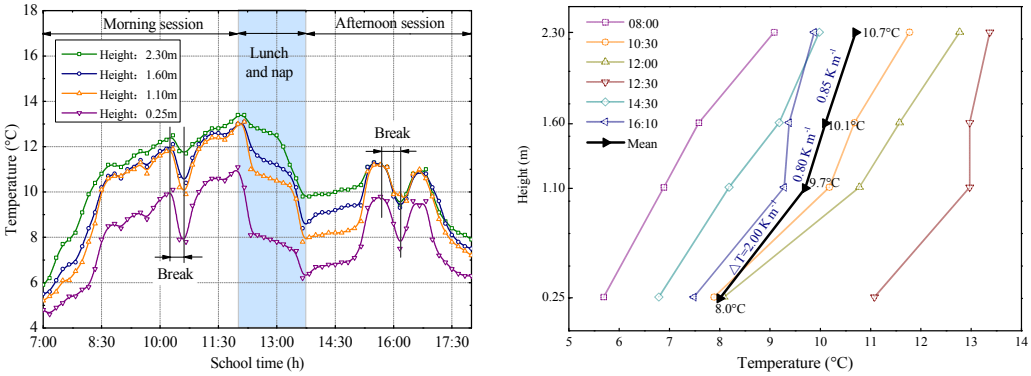

(a) Temperature variation (b) Temperature distribution at different times

Fig. 3: Temperature distribution in vertical direction

Horizontal temperature distribution. The temperature at the south measuring point was generally higher than the north. The average value was 11.4°C, 10.9°C, 10.8°C and 10.7°C from south to north in turns. It can be seen from Fig.4 (a). that the tendency of the temperature distribution was generally similar except for the curve at P9. Because the P9 point was located in the south, the influence of solar radiation was the strongest. From 16:00 to 17:00, the temperature at P9 rose sharply.

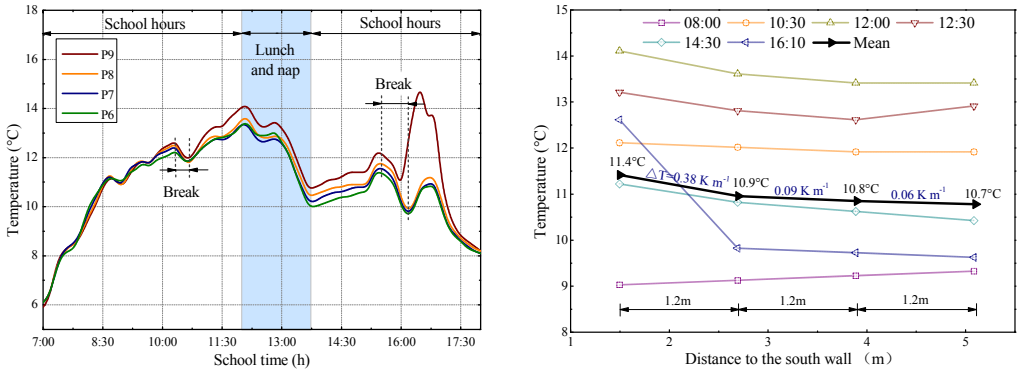

(a) Temperature variation (b) Temperature distribution at different times

Fig. 4: Temperature distribution in horizontal direction

The temperature values at different points are shown in Fig. 4(b). It can be seen that the tendency of the temperature distribution was generally similar except at 8:00 and 16:10. At 8:00, the temperature elevated from south to north due to less solar radiation. With the increase of solar radiation, the temperature increased rapidly at the south end of the room. At 16:10, the temperature at south rises sharply. The differences between the northern and southern temperatures are caused by the increased heat loss on the north side due to differences on both sides of the outdoor environment temperature in the winter and the increased solar radiation heat gain in

the south. Based on the above, solar radiation intensity plays a decisive role in the south - north temperature distribution differences.

3.2. Model validation

To verify the differences between the measured and simulated results and verify the reliability of the simulation and the measurements, a comparative analysis of the measured and simulated temperature values between 1.1 m and 1.6 m are shown in Fig. 5. It can be seen that the simulated temperatures at each measurement position concurred with the experimental temperatures, with the same trend over the measurement period. For example, the temperature tendencies of the measurement and the simulation at P3 in the morning and at P4 in the afternoon are shown in Fig. 5(a) and Fig. 5(b), respectively. It can be seen that the mean simulated results were higher than the measured results by 0.3°C to 0.4°C; the mean simulated and measured temperatures at P3 in the morning were 11.7°C and 11.3°C, and the mean simulated and measured temperatures at P4 in the afternoon were 9.9°C and 9.6°C, respectively. This small difference was caused by objective factors. Although the simulation closely adheres to the actual situation, there are certain simplifications that cannot be fully considered such as various indoor objects and accidental disturbances. In addition, the specific locations of the actual measuring points are not precisely the same as the simulation locations.

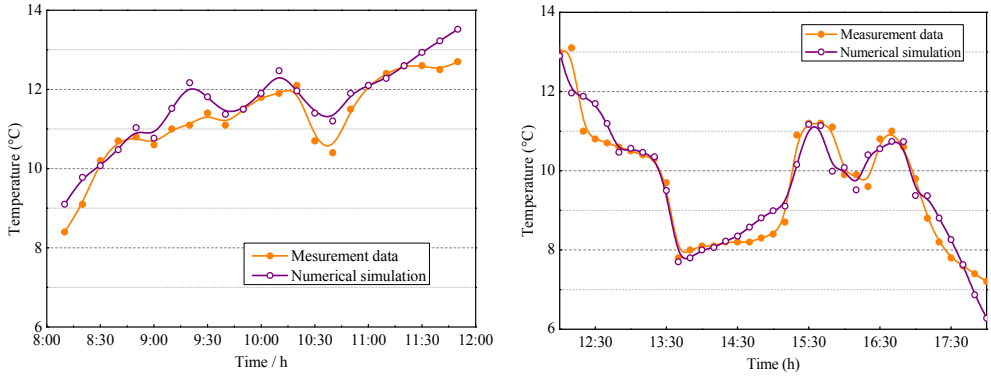

(a) Verification of P3 at 1.6m in the morning (b) Verification of P4 at 1.1m in the afternoon

Fig. 5: Comparison of the temperature distribution obtained by simulation and in-situ measurements

3.3. Simulated temperature distribution

Different solar radiation intensity levels. Fig. 6(a) shows the temperature changes of different positions at a height of 1.1m. The temperature at the same location essentially shows a linearly increasing trend with increasing solar radiation intensity. The temperature amplification differs with the increase of solar radiation at different locations from the south wall; the closer to the south wall, the greater the slope of increased temperature. The temperature increased by 2.3°C, 2.1°C and 1.9°C from distances of 0.8m, 3.3m and 5.8m to the south wall, respectively, when the solar radiation increased in100 W m^{-2} increments. At 3.3 m from the south wall, the temperature increased by 14.7°C when the solar radiation increased from 100 W m^{-2} to 800 W m^{-2}. The temperature increased by 0.7°C and 1.0°C at different locations from distances of 0.8m to 3.3m and from distances of 3.3m to 5.8m at a solar radiation of 600 W m^{-2}. The temperature gradient is lower when closer to the south wall and greater when further away.

Different thicknesses of south external wall. The simulation was carried out under the following conditions: a solar radiation of 600 W m^{-2}, a window-to-wall area ratio of 0.3, and a time of 12 noon. Fig. 6(b) shows the temperature changes of different positions at height of 1.1m.The temperature at the same location shows a trend of initial decrease and subsequent increase with the increase of south wall thickness. When the wall thickness is increased from 260mm to 390mm, the temperature significantly decreases by 5°C at 3.3 m distance to the south wall. When the wall thickness is increased from 390mm to 540mm, temperature slightly decreases by less by 1°C. When it increased from 540mm to 650mm, the temperature only decreases by 0.2°C. In short, the impact on indoor temperature is significant with increasing south wall thickness, but the indoor temperature will eventually rise when the wall thickness increases to a certain extent.

Different window-to-wall area ratios. The simulation was carried out under the following conditions: a solar radiation of 600 W m^{-2}, a 540-mm south wall thickness, and a time of and 12 noon. Fig. 6(c) shows the temperature changes of different positions at height of 1.1m. The temperature at the same location essentially

showed an increasing trend with the increased window-to-wall area ratios. The temperature growth trends differed with the increase of the window-to-wall area ratio at different positions to the south wall. At 0.8m from the south wall, the temperature increase was greater with an area ratio of 0.3 to 0.4 and more gradual with an area ratio of 0.4 to 0.7; the further from the south wall, the more gradual the temperature variation. This may be due to an increase in the area of the window. The window increases the quantity of heat but simultaneously contributes to heat loss because it is poorly constructed for heat gain and loss reduction.

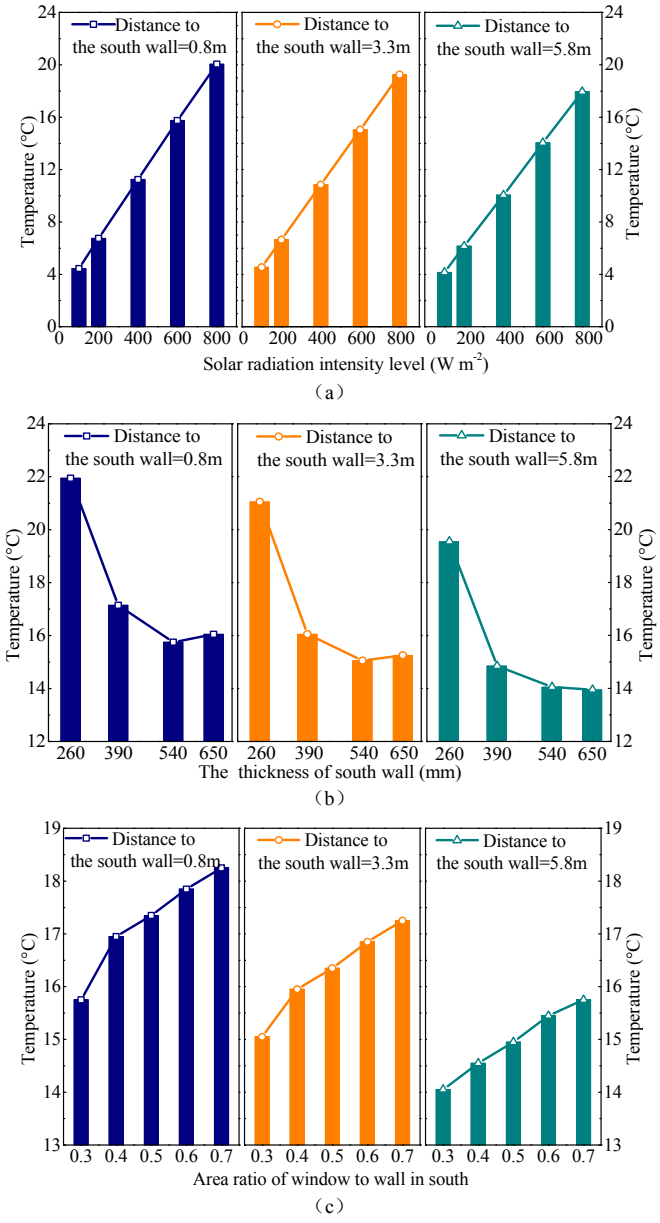

Fig. 6: The evolution of temperature distribution under different simulation cases

4. Conclusions

A computer simulation model using the finite-volume-based commercial software Fluent was used to evaluate classroom temperature distributions. Experiments were conducted in an experimental primary school classroom in northwestern China to validate the simulation model. The simulated results concurred with the measured temperatures. The validated computer simulation model was applied to predict classroom temperature distributions with various conditions. The following conclusions were obtained:

(1) Based on the measured temperature data, there is significant non-uniformity in the temperature field

distribution inside the measured building. The vertical direction of the average air temperature in the classroom was nearly 3.0°C; the horizontal direction of the average temperature was approximately 1.0°C.

(2) Within the range of 0.25m to 1.10m in vertical direction, the temperature gradient was approximately 2.0 °C m^{-1}, whereas the temperature gradient was reduced to 0.8 °C m^{-1} at 1.10 to 2.30m. The closer to the south wall, the more obvious the temperature difference in horizontal direction. From 1.5m to 2.7m, 2.7m to 3.9m, and 3.9m to 5.1m, the temperature gradients were 0.38, 0.09 and 0.06 °C m^{-1}, respectively.

(3)The simulated results showed that the indoor temperature changed when the solar radiation intensity was varied; the temperature trends were linear. The temperature gradient is lower when closer to the south wall and greater when further away.

(4)The indoor temperature changed when the thickness of the south wall was varied and the temperature trends were non-linear. The temperature at the same location shows a trend of initial decrease and subsequent increase with the increase of south wall thickness. So a thinner south wall was preferable.

(5)The indoor temperature changed when the window-to-wall area ratio was varied, and the temperature at the same location essentially showed an increasing trend. At different positions, however, the temperature growth trends differed with an increase of window-to-wall area ratio; the further the distance from the south wall, the more gently the temperature varied.

Acknowledgements

The research was supported by the National Key Research Project (Project No. 2016YFC0700400), and the National Natural Science Foundation of China (Project Nos. 51678468 and 51590911).

References

Behnia, M., Reizes, J.A., Davis, G., 1990. Combined radiation and natural convection in a cavity with a transparent wall and containing a non-participant fluid. Int J Numer Meth Fl. 10, 3205-3225.

Berdahl, P., Fromberg, R.,1982. The thermal radiance of clear skies. Sol Energy. 29, 299-314.

Catalina, T., Virgone, J., Kuznik, F., 2009. Evaluation of thermal comfort using combined CFD and experimentation study in a test room equipped with a cooling ceiling. Build Environ. 44, 1740-1750.

Cheng, K.W.D., Djunaedy, E., Chua, Y.I., Tham, K.W., Sekhar, S.C., Wong, N.H., Ullan, M.B., 2003. Thermal comfort study of an air-conditioned lecture theatre in the tropics. Build Environ. 38, 63-73.

Cook, J., 1985. Passive Cooling. MIT Press, Cambridge.

Corgnati, S.P., Filippi, M., Viazzo, S., 2007. Perception of the thermal environment in high school and university classrooms: Subjective preferences and thermal comfort. Build Environ. 42, 951-959.

Corrado, V., Astolfi, A.,2002. Environmental quality assessment of classrooms. In: Proceedings of EPIC 2002 AIVC international conference, Lyon, 251-256.

Desta, T.Z., Janssens, K.,2004. CFD for model-based controller development. Build Environ. 39, 621-633.

Havenith, G.,2007. Metabolic rate and clothing insulation data of children and adolescents during various school activities. Ergonomics. 50, 1689-1701.

Ismail, K.A.R., Henriquez, J.R.,2003. Modeling and simulation of a simple glass window. Sol Energ Mat Sol C. 80, 355-374.

Molina-Aiz, F.D., Ftnassi, H., Boulard, T., Roy, J.C., Valera, D.L.,2010. Comparison of finite element and finite volume methods for simulation of natural ventilation in greenhouses. Comput Electron Agr. 72, 69-86.

Rohdin, P., Moshfegh, B., 2007. Numerical predictions of indoor climate in large industrial premises a comparison between different κ-ε models supported by field measurements. Build Environ. 42, 3872-3882.

Rundle, C., Lightstone, M., Osthuizen, P., 2011. Validation of computational fluid dynamics simulations for atria geometries. Build Environ. 46, 1343-1353.

Srebric, J., Vukovic, V., He, G., Yang, X.,2008. CFD boundary conditions for contaminant dispersion, heat transfer and airflow simulations around human occupants in indoor environments. Build Environ. 43, 294-303.

Stamou, A., Katsiris, I., 2006. Verification of a CFD model for indoor airflow and heat transfer. Build Environ. 41, 1171-1181.

Tang, R.S., Meir, I.A., Etzion, Y.,2003. Thermal behavior of buildings with curved roofs as compared with flat roofs. Sol Energy. 74, 273-286.

Valeria, D.G., Osvaldo, D.P., Michele, D.C., 2012. Indoor environmental quality and pupil perception in Italian primary schools. Build Environ. 56, 335-345.

Versteeg, H.K., Malalasekera, W., 1995. An introduction to computational fluid dynamics. Longman Group Ltd, London.

Zhang, X., Wang, H.L., Zou, Z.R., Wang, S.J., 2016. CFD and weighted entropy based simulation and optimisation of Chinese Solar Greenhouse temperature distribution. Biosyst Eng. 142, 12-26.